

Bifurcations and patterns in the Kuramoto model with inertia

Hayato Chiba*, Georgi S. Medvedev† and Matthew S. Mizuhara‡

June 8, 2023

Abstract

In this work, we analyze the Kuramoto model (KM) with inertia on a convergent family of graphs. It is assumed that the intrinsic frequencies of the individual oscillators are sampled from a probability distribution. In addition, a given graph, which may also be random, assigns network connectivity. As in the original KM, in the model with inertia, the weak coupling regime features mixing, the state of the network when the phases (but not velocities) of all oscillators are distributed uniformly around the unit circle. We study patterns, which emerge when mixing loses stability under the variation of the strength of coupling. We identify a pitchfork (PF) and an Andronov-Hopf (AH) bifurcations in the model with multimodal intrinsic frequency distributions. To this effect, we use a combination of the linear stability analysis and Penrose diagrams, a geometric technique for studying stability of mixing. We show that the type of a bifurcation and a nascent spatiotemporal pattern depend on the interplay of the qualitative properties of the intrinsic frequency distribution and network connectivity.

1 Introduction

In this paper, we study the following system of coupled second order damped oscillators on a convergent sequence of graphs $\{\Gamma_n\}$:

$$\ddot{\theta}_i + \gamma \dot{\theta}_i = \omega_i + \frac{2K}{n} \sum_{j=1}^n a_{ij}^n \sin(\theta_j - \theta_i), \quad i \in [n] := \{1, 2, \dots, n\}, \quad (1.1)$$

where $\theta_i : \mathbb{R}^+ \rightarrow \mathbb{T} := \mathbb{R}/2\pi\mathbb{Z}$ denotes the phase of the i th oscillator, $\gamma > 0$ is a damping constant, K is the coupling strength and a_{ij}^n is the adjacency matrix of Γ_n . Intrinsic frequencies $\omega_i, i \in [n]$, are independent identically distributed random variables drawn from the probability distribution with density g . By rescaling time, intrinsic frequencies, and K , one can make $\gamma = 1$, which will be assumed without loss of generality throughout this paper.

*Advanced Institute for Materials Research, Tohoku University, Sendai, 980-8557, Japan, hchiba@tohoku.ac.jp

†Department of Mathematics, Drexel University, 3141 Chestnut Street, Philadelphia, PA 19104, medvedev@drexel.edu

‡Department of Mathematics and Statistics, The College of New Jersey, mizuham@tcnj.edu

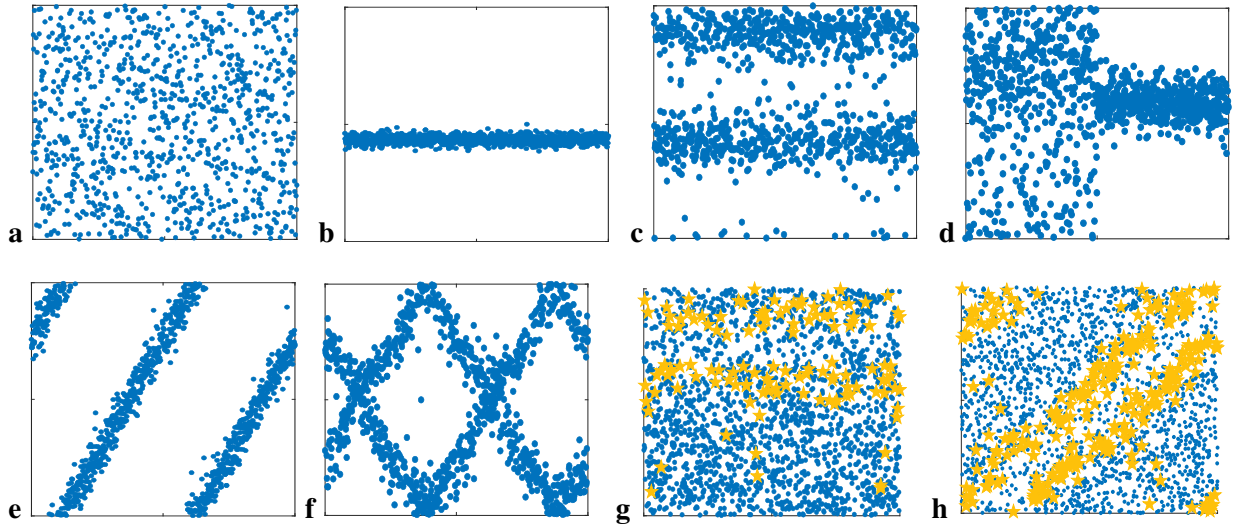


Figure 1: A collection of patterns generated by (1.1) with unimodal and bimodal frequency distributions on complete and nonlocal nearest-neighbor graphs: a) mixing, b) synchronization, c) clusters, d) chimeras, e) twisted states, f) two sets of twisted states traveling in opposite directions, g) a two-cluster partially locked state, h) a two-cluster twisted partially locked state. In g) and h) yellow stars correspond stationary clusters superimposed onto irregularly moving oscillators. Patterns in a)-f) can also be generated using a classical (first order) Kuramoto model using the same settings (cf. [18]). Patterns in g) and h) are new. Unless otherwise stated, all simulations of (1.1) were performed with $n = 10^3$ and $\gamma = 1$. The snapshots **b-h** are representative for the dynamical states bifurcating from the incoherent state shown in **a**. The range of K and the network connectivity corresponding to these patterns are explained in the text and in the bifurcation diagrams below.

The system of equations (1.1) is a generalization of the KM of coupled phase oscillators, which provides an important framework for studying collective dynamics in coupled networks [15, 20]. This is also an established model of a power network [10, 21, 25]. The second order derivatives are used to incorporate inertial effects into the system's dynamics. Thus, the name - the KM with inertia. Compared to the original KM, it is a more flexible model with more degrees of freedom and richer dynamics. It features a range of spatiotemporal patterns found in the original KM [7, 18] as well as a few new ones that have not been studied before (Figure 1).

The KM is best known for the phase transition from a highly irregular mixing behavior in the weak coupling regime to a gradual buildup of coherence leading to synchronization [15, 23]. In the first order KM with intrinsic frequencies sampled from a symmetric unimodal distribution, the transition to synchrony lies through the pitchfork (PF) bifurcation of mixing [2, 8]. A similar mechanism is involved in the transition to synchronization in the KM on graphs [4, 6]. In the KM with more general coupling functions or with multimodal frequency distribution mixing may lose stability through the Andronov-Hopf (AH) bifurcation [3, 7, 18]. Qualitative properties of the intrinsic frequency distribution and the properties of network topology translate into a variety of spatiotemporal patterns replacing mixing when it loses stability [7, 18]. Following [7, 18], we use a combination of the linear stability analysis [5] and Penrose diagrams [8, 18, 19] to describe bifurcations leading to the loss of stability of mixing as well as emerging patterns in the KM with inertia. We find many parallels in pattern formation mechanisms involved in both the ordinary KM and the KM with inertia, but we also find patterns that are not present in the former model. For instance, we identified a class of partially locked states (PLS) based on stationary antiphase clusters (cf. [17]) (see Fig. 1 **g, h**). We show that the KM with inertia with symmetric bimodal (with well separated peaks) frequency distribution and nonlocal nearest neighbor coupling has four distinct bifurcation scenarios (cf. (5.3)), compared to a single one for the ordinary KM in a similar setting (see Section 5). Overall, the KM with inertia offers a richer repertoire of patterns.

The loss of stability of the incoherent state in the KM with inertia on with all-to-all coupling was studied in [1, 12, 13, 24]. The results in these papers are based on self-consistent analysis and numerical simulations. Our approach relies on a rigorous linear stability analysis and applies to the KM with multimodal frequency distributions on convergent graph sequences. We show that the loss of stability of the incoherent state may lead to a variety of interesting spatiotemporal patterns, which can be related to the qualitative properties of the intrinsic frequency distribution and network topology.

The paper is organized as follows. The next section presents necessary information about stability of mixing adapted from [5]. In Section 3, we analyze the loss of stability of mixing in the model with a unimodal intrinsic frequency distribution. We use this problem as a convenient setting to introduce Penrose diagrams. The full power of this technique is revealed when we apply it to study bifurcations in the model with a family of bimodal intrinsic frequency distributions in Section 4. Here, in addition, to the PF bifurcation of mixing which already appeared in the unimodal case, we encounter an AH bifurcation. The latter is responsible for formation of traveling clusters. Furthermore, we describe another PF bifurcation, which occurs at a negative value of K . In contrast to the PF in the model with unimodal distribution, this time the PF bifurcation supports stationary antiphase clusters superimposed onto irregularly moving oscillators. This pattern was not present in the ordinary KM in (cf [18]). In Section 5, we describe the role of the network topology on patterns emerging when mixing loses stability. We end this paper with concluding remarks in Section 6.

2 The linear stability of mixing

2.1 The mean field limit

The first step in the analysis of mixing is the derivation of the mean field limit for (1.1). To this end, we rewrite (1.1) as follows

$$\begin{aligned}\dot{\theta}_i &= \psi_i + \omega_i, \\ \dot{\psi}_i &= -\psi_i + \frac{2K}{n} \sum_{j=1}^n a_{ij}^n \sin(\theta_j - \theta_i), \\ \dot{\omega}_i &= 0, \quad i \in [n].\end{aligned}\tag{2.1}$$

Equation (2.1) shows that the phase space of each (uncoupled) oscillator is $\mathbb{T} \times \mathbb{R} \times \mathbb{R}$. With (2.1) at hand, it is straightforward to write down the Vlasov equation describing the dynamics of (2.1) in the limit as $n \rightarrow \infty$ (cf. [11])

$$\partial_t f + \partial_\theta ((\psi + \omega) f) + \partial_\psi ((-\psi + \mathbf{N}[f]) f) = 0,\tag{2.2}$$

where

$$\mathbf{N}[f](t, \theta, x) = \frac{K}{i} \left(e^{-i\theta} h(t, x) - e^{i\theta} \overline{h(t, x)} \right)$$

and

$$h(t, x) = \int_{\mathbb{T} \times \mathbb{R}^2 \times I} W(x, y) e^{i\theta} f(t, \theta, \psi, \omega, y) d\theta d\psi d\omega dy,\tag{2.3}$$

is the local order parameter. Here, $I = [0, 1]$ and $f(t, \theta, \psi, \omega, x) d\theta d\psi d\omega$ stands for the probability that the state of the oscillator at the ‘spatial’ location $x \in I$ and time $t \geq 0$ is in $[\theta, \theta + d\theta) \times [\psi, \psi + d\psi) \times [\omega, \omega + d\omega)$. W is a square integrable function on I^2 , which describes the limit of the graph sequence $\{\Gamma_n\}^1$.

A distribution-valued solution $f(t, \theta, \psi, \omega, x)$ of the initial value problem for the Vlasov equation (2.2) yields the probability distribution of particles in the phase space $\mathbb{T} \times \mathbb{R}^2$ for each $(t, x) \in \mathbb{R}^+ \times I$ (cf. [9, 14]). By mixing we mean the following steady state solution of (2.2)

$$f_{mix} = \frac{g(\omega)}{2\pi} \delta(\psi),\tag{2.4}$$

where δ stands for Dirac’s delta function. f_{mix} corresponds to the stationary regime, which is characterized by the uniform distribution of the phases $\theta_i, i \in [n]$.

2.2 The linearized equation

In this section, we present the key steps in the stability analysis and refer the reader to [5] for more details.

Throughout this paper, we will assume the following.

¹Such functions are called graphons in the graph theory. For the details on graphons, graph limits, and their applications to the continuum description of the dynamical networks, we refer the interested reader to [4, 16].

Assumption 2.1. Let g be a real analytic function. In addition, we assume that $\hat{g}(\eta) := \int_{\mathbb{R}} e^{i\eta\omega} g(\omega) d\omega$ is a continuous function such that

$$\lim_{\eta \rightarrow \infty} |\hat{g}(\eta)| e^{a\eta} = 0 \quad (2.5)$$

for some $0 < a < 1$.

Remark 2.2. By the Paley-Wiener theorem, (2.5) implies that $g(\omega)$ has an analytic continuation to the region $0 \leq \text{Im}(z) < a$.

Since ω does not change in time, f satisfies the following constraint

$$g(\omega) = \int_{\mathbb{T} \times \mathbb{R}} f(t, \theta, \psi, \omega, x) d\theta d\psi, \quad \forall (t, x) \in \mathbb{R}^+ \times I. \quad (2.6)$$

Next, we recast (2.2) in Fourier variables

$$\partial_t u_j = (j - \zeta) \partial_\zeta u_j + j \partial_\eta u_j + K \zeta (h(t, x) u_{j-1} - \overline{h(t, x)} u_{j+1}), \quad j \in \mathbb{Z}, \quad (2.7)$$

where we used

$$u_j(t, \zeta, \eta, x) = \int_{\mathbb{R}^2 \times \mathbb{T}} e^{i(j\theta + \zeta\psi + \eta\omega)} f(t, \theta, \psi, \omega, x) d\theta d\psi d\omega, \quad j \in \mathbb{Z} \quad (2.8)$$

and integration by parts. Note that the expression for the local parameter can be rewritten as

$$h(t, x) = \int_I W(x, y) u_1(t, 0, 0, y) dy.$$

In addition, we have the following constraints

$$u_0(t, 0, 0, x) = 1, \quad (2.9)$$

$$u_{-j}(t, -\zeta, -\eta, x) = \overline{u_j(t, \zeta, \eta, x)}, \quad j \in \mathbb{N}. \quad (2.10)$$

Equation (2.9) follows from (2.6). Equation (2.10) follows from the fact that f is real. Thus, it is sufficient to restrict to $j \in \mathbb{N} \cup \{0\}$ in (2.7).

By changing from ζ to ξ given by the following relations:

$$\begin{cases} \zeta - j = -e^{-\xi_j}, & \zeta - j < 0, \\ \zeta - j = e^{-\xi_j}, & \zeta - j \geq 0, \end{cases} \quad (2.11)$$

and setting

$$v_j(t, \xi_j, \eta, x) := \begin{cases} u_j(t, j - e^{-\xi_j}, \eta, x), & \zeta - j < 0, \\ u_j(t, j + e^{-\xi_j}, \eta, x), & \zeta - j \geq 0, \end{cases} \quad (2.12)$$

we obtain

$$\partial_t v_j = \partial_{\xi_j} v_j + j \partial_\eta v_j + K (j - e^{-\xi_j}) \left(h(t, x) v_{j-1} - \overline{h(t, x)} v_{j+1} \right), \quad j \in \mathbb{Z} \quad (2.13)$$

$$h(t, x) = \int_I W(x, y) v_1(t, 0, 0, y) dy, \quad (2.14)$$

subject to the constraint $\lim_{\xi \rightarrow \infty} v_0(t, \xi, \eta, x) = \hat{g}(\eta)$. For $j \geq 0$, we adopt the first line of (2.11) because in the definition of the local order parameter, we need $u_1(t, 0, 0, x)$, for which $\zeta - j = -1 < 0$. By the same reason, we use the second line for $j \leq -1$.

The steady state of the Vlasov equation, f_{mix} , in the Fourier space has the following form

$$v_0 = \hat{g}(\eta), \quad v_j = 0, j \in \mathbb{N}. \quad (2.15)$$

To investigate the stability of (2.15), let $w_0 = v_0 - \hat{g}(\eta)$ and $w_j = v_j$ for $j \neq 0$. Then we obtain the system

$$\begin{cases} \partial_t w_1 = \partial_{\xi_1} w_1 + \partial_{\eta} w_1 + K(1 - e^{-\xi_1}) \left(h(t, x) \hat{g}(\eta) + h(t, x) w_0 - \overline{h(t, x)} w_2 \right), \\ \partial_t w_j = \partial_{\xi_j} w_j + j \partial_{\eta} w_j + K(j - e^{-\xi_j}) \left(h(t, x) w_{j-1} - \overline{h(t, x)} w_{j+1} \right), \quad j \geq 0 \text{ and } j \neq 1, \\ h(t, x) = \int_I W(x, y) w_1(t, 0, 0, y) dy, \end{cases} \quad (2.16)$$

and $\lim_{\xi \rightarrow \infty} w_0(t, \xi, \eta, x) = 0$. Our goal is to investigate the stability and bifurcations of the steady state (mixing) $w_j = 0, j \in \mathbb{Z}$ of this system.

The linearized system has the following form

$$\partial_t w_1 = \mathbf{L}_1[w_1] + K \mathbf{B}[w_1] =: \mathbf{S}[w_1], \quad (2.17)$$

$$\partial_t w_j = \mathbf{L}_j[w_j], \quad j \geq 0 \text{ and } j \neq 1, \quad (2.18)$$

where

$$\mathbf{L}_j[\phi](\xi, \eta, x) = (\partial_{\xi} + j \partial_{\eta}) \phi(\xi, \eta, x), \quad j \in \mathbb{Z} \quad (2.19)$$

$$\mathbf{B}[\phi](\xi, \eta, x) = (1 - e^{-\xi}) \hat{g}(\eta) \mathbf{W}[\phi(0, 0, \cdot)](x), \quad (2.20)$$

and

$$\mathbf{W}[f](x) = \int_{\mathbb{R}} W(x, y) f(y) dy. \quad (2.21)$$

The self-adjoint operator \mathbf{W} reflects the impact of connectivity on stability of mixing.

2.3 The spaces

To proceed with the linear stability analysis of the mixing state, we need to introduce the following Banach spaces.

Recall $a \in (0, 1)$ defined in Assumption 2.1. For $\alpha \in \{0, 1\}$, let

$$\beta_1^+(\eta) = \max\{1, e^{\alpha\eta}\}, \quad \beta_1^-(\eta) = \min\{1, e^{\alpha\eta}\}, \quad \text{and} \quad \beta_2(\xi) = \min\{e^{\xi}, 1\}, \quad (2.22)$$

and define

$$\begin{aligned}\mathcal{X}_\alpha^\pm &= \{\phi : \text{continuous on } \mathbb{R}, \|\phi\|_{\mathcal{X}_\alpha^\pm} = \sup_\eta \beta_1^\pm(\eta) |\phi(\eta)| < \infty\}, \\ \mathcal{Y}_\alpha^\pm &= \{\phi : \text{continuous on } \mathbb{R}^2, \|\phi\|_{\mathcal{Y}_\alpha^\pm} = \sup_{\xi, \eta} \beta_1^\pm(\eta) \beta_2(\xi) |\phi(\xi, \eta)| < \infty\}, \\ \mathcal{H}_\alpha^\pm &= L^2(I; \mathcal{Y}_\alpha^\pm).\end{aligned}\tag{2.23}$$

Recall that I stands for $[0, 1]$. The norms on \mathcal{H}_α^\pm are defined by

$$\|\phi\|_{\mathcal{H}_\alpha^\pm}^2 = \int_I \left(\sup_{\xi, \eta} \beta_1^\pm(\eta) \beta_2(\xi) |\phi(\xi, \eta, x)| \right)^2 dx.\tag{2.24}$$

Note that the spaces

$$\mathcal{H}_a^+ \subset \mathcal{H}_0^+ = \mathcal{H}_0^- \subset \mathcal{H}_a^-$$

form a Gelfand triplet. Since the linear operators defined above have essential spectra on the imaginary axis, we need the generalized spectral theory based on the Gelfand triplet to detect bifurcations of mixing [5].

2.4 The spectrum of S

Recall the definition of W (2.21) and note that it is a compact self-adjoint operator on $L^2(I)$. Therefore, the eigenvalues of W are real with the only accumulation point at 0. We denote the set of eigenvalues of W by $\sigma_p(W)$.

Operators $L_j, j \in \mathbb{Z}$ and B are densely defined on \mathcal{H}_0^+ (see (2.19), (2.20)) and B is a bounded operator (cf. [5]). The resolvent of L_j is given by

$$(\lambda - L_j)^{-1}[v](\xi, \eta, x) = \begin{cases} \int_0^\infty e^{-\lambda t} v(\xi + t, \eta + jt, x) dt, & \Re \lambda > 0, \\ -\int_{-\infty}^0 e^{-\lambda t} v(\xi + t, \eta + jt, x) dt & \Re \lambda < 0. \end{cases}\tag{2.25}$$

The right-hand side of (2.25) belongs to \mathcal{H}_0^+ for any $v \in \mathcal{H}_0^+$ only if $\Re \lambda < -1$ or $\Re \lambda > 0$. For $-1 \leq \Re \lambda \leq 0$, the set of v such that the right-hand side exists is not dense in \mathcal{H}_0^+ . Thus, the residual spectrum of L_j is the region $\mathbb{S}_1 := \{z \in \mathbb{C} : -1 \leq \Re z \leq 0\}$. \mathbb{S}_1 contains no eigenvalues of $L_j, j \in \mathbb{Z}$. The essential spectrum of S is given by \mathbb{S}_1 , because $S = L_1 + KB$ is the bounded perturbation of L_1 . However, \mathbb{S}_1 may still contain eigenvalues of S , as one can see from the following lemma.

Lemma 2.3. (cf. [5]) *Let ν be a nonzero eigenvalue of W and let $V_\nu \in L^2(I)$ be a corresponding eigenfunction. Define*

$$D(\lambda, \xi, \eta) = \int_{\mathbb{R}} \left(\frac{1}{\lambda - i\omega} - \frac{e^{-\xi}}{\lambda + 1 - i\omega} \right) e^{i\eta\omega} g(\omega) d\omega,\tag{2.26}$$

and

$$G(\lambda) := D(\lambda, 0, 0) = \int_{\mathbb{R}} \left(\frac{1}{\lambda - i\omega} - \frac{1}{\lambda + 1 - i\omega} \right) g(\omega) d\omega.\tag{2.27}$$

Then the root $\lambda = \lambda(\nu)$ of the following equation

$$G(\lambda) = \frac{1}{K\nu}, \quad (2.28)$$

not belonging to $\partial\sigma(\mathbf{L}_1) = \{z \in \mathbb{C} : \Re z = -1 \text{ or } \Re z = 0\}$, is an eigenvalue of \mathbf{S} on \mathcal{H}_0^+ . For each such root $\lambda = \lambda(\nu)$ the corresponding eigenfunction is given by

$$v_\lambda(\xi, \eta, x) = D(\lambda, \xi, \eta)V_\nu(x). \quad (2.29)$$

To study patterns arising at the bifurcations of mixing we define the function

$$\Upsilon_\lambda(\omega, \xi) = \left(\frac{1}{\lambda - i\omega} - \frac{e^{-\xi}}{\lambda + 1 - i\omega} \right) g(\omega). \quad (2.30)$$

Then, the following equality holds:

$$v_\lambda(\xi, \eta, x) = F_\eta[\Upsilon_\lambda](\xi, \eta)V_\nu(x), \quad (2.31)$$

where F_η is the Fourier transform with respect to $\omega \mapsto \eta$.

Let

$$\mathbb{H}_a := \{z \in \mathbb{C} : \Re z > -a\}. \quad (2.32)$$

For $\Re \lambda > 0$, $\Upsilon_\lambda(\omega, \xi)$ is an integrable function in ω as can be seen from (2.30). For $\lambda = iu \in i\mathbb{R}$, $\Upsilon_\lambda(\omega, \xi)$ is no longer an integrable function, but it can be interpreted as a tempered distribution, as the following argument shows. By Sokhotski–Plemelj formula (cf. [22]), we have

$$\begin{aligned} \lim_{x \rightarrow 0+} \langle \Upsilon_{x+iy}, \phi \rangle &= \lim_{x \rightarrow 0+} \int_{-\infty}^{\infty} \frac{g(\omega)\phi(\omega)}{x + iy - i\omega} d\omega - \int_{-\infty}^{\infty} \frac{e^{-\xi}g(\omega)\phi(\omega)}{1 + i(y - \omega)} d\omega \\ &= \pi g(y)\phi(y) + i \text{ p.v.} \int_{-\infty}^{\infty} \frac{g(\omega + y)\phi(\omega + y)}{\omega} d\omega - \int_{-\infty}^{\infty} \frac{e^{-\xi}g(\omega)\phi(\omega)}{1 + i(y - \omega)} d\omega, \end{aligned}$$

for any ϕ from the Schwartz class $\mathcal{S}(\mathbb{R})$. Thus, $\Upsilon_{iy} := \lim_{x \rightarrow 0+} \Upsilon_{x+iy} \in \mathcal{S}'(\mathbb{R})$ for each ξ and

$$\Upsilon_{iy} = \pi g(y)\delta_y + i\mathcal{P}_y[g] - \frac{e^{-\xi}g(\omega)}{1 + i(y - \omega)}, \quad (2.33)$$

where δ_y stands for the Dirac's delta function supported at y and

$$\langle \mathcal{P}_y[g], \phi \rangle = \text{p.v.} \int_{-\infty}^{\infty} \frac{g(\omega + y)\phi(\omega + y)}{\omega} d\omega. \quad (2.34)$$

Indeed, $\lim_{\lambda \rightarrow 0+} v_\lambda(\xi, \eta, x)$ is an element of the space \mathcal{H}_a^- , the dual space of \mathcal{H}_a^+ . This fact was used to apply the center manifold reduction on \mathcal{H}_a^- in [5].

The formulae for eigenfunctions of \mathbf{S} (2.31)-(2.33) corresponding to bifurcating eigenvalues will be used below to explain spatiotemporal patterns arising at the loss of stability of mixing.

3 The method of Penrose

Having reviewed the linear stability analysis, we next focus on the instability of mixing. To this end, we use a geometric method for locating and identifying bifurcations in the Vlasov equation, which was invented by Penrose in the context of Landau damping [19]. This method was adapted to the analysis of the classical Kuramoto model in [8] and the Kuramoto model on graphs in [7, 18].

In this section, we explain Penrose's method by applying it to the second order model (1.1) with a unimodal density (see Fig. 2a). In the next section, we apply this method to unfold a codimension-2 bifurcation of mixing in the model with a bimodal density. In these two sections, we restrict to $W \equiv 1$, which corresponds to the all-to-all connectivity. The bifurcation scenarios discussed below will also hold for the KM on any graph sequence with a constant graph limit, e.g., Erdős-Rényi or Paley graphs [6].

For $W \equiv 1$, the only nonzero eigenvalue of \mathbf{W} is $\nu = 1$ of multiplicity 1. Thus, the equation for the eigenvalues of \mathbf{S} (2.28) takes the following form

$$G(\lambda) = K^{-1}, \quad (3.1)$$

where G is defined in (2.27).

Our goal is to locate the roots of (3.1) in $\mathbb{H}_0 = \{\lambda \in \mathbb{C} : \Re \lambda > 0\}$ and find a bifurcation value $K = K_c$ at which the root disappears from \mathbb{H}_0 . To this end, we introduce

$$G(iy) = \lim_{x \rightarrow 0+} G(x + iy)$$

and denote $\mathcal{C} = \{G(it) \in \mathbb{C} : t \in \mathbb{R}\}$. The Sokhotski-Plemelj formula [22] gives

$$\begin{aligned} G(it) &= \pi g(t) - \int_{-\infty}^{\infty} \frac{g(\omega)}{1 + (\omega - t)^2} d\omega \\ &\quad + i \left\{ \int_0^{\infty} \frac{g(t + \omega) - g(t - \omega)}{\omega} d\omega - \int_{-\infty}^{\infty} \frac{(\omega - t)g(\omega)}{1 + (\omega - t)^2} d\omega \right\}. \end{aligned} \quad (3.2)$$

This yields the following parametric equations for \mathcal{C} :

$$\begin{aligned} x &= \pi g(t) - \int_{-\infty}^{\infty} \frac{g(\omega)}{1 + (\omega - t)^2} d\omega, \\ y &= \int_0^{\infty} \frac{g(t + \omega) - g(t - \omega)}{\omega} d\omega - \int_0^{\infty} \frac{\omega (g(t + \omega) - g(t - \omega))}{1 + \omega^2} d\omega \\ &= \int_0^{\infty} \frac{g(t + \omega) - g(t - \omega)}{\omega(1 + \omega^2)} d\omega \end{aligned} \quad (3.3)$$

for $t \in \mathbb{R}$. Note that $(x, y) \rightarrow 0$ as $t \in \pm\infty$. Thus, \mathcal{C} is a bounded closed curve.

Next, suppose g is an even unimodal density (see Fig. 2a). The even symmetry of g implies that \mathcal{C} is symmetric about the x -axis (cf. (3.3)). It intersects the positive real semiaxis at a unique point $P_0 = (x_0, 0)$, $x_0 > 0$. Further, note that $G(0) = x_0$ (Figure 2a, b). From the x -equation in (3.3) we find

$$x_0 = \pi g(0) - \int_{-\infty}^{\infty} \frac{g(\omega)}{1 + \omega^2} d\omega = \int_{-\infty}^{\infty} \frac{g(0) - g(\omega)}{1 + \omega^2} d\omega > 0. \quad (3.4)$$

Define

$$K_c := (x_0)^{-1}. \quad (3.5)$$

By the Argument Principle, the number of roots of (3.1) in \mathbb{H}_0 is equal to the winding number of \mathcal{C} about K^{-1} [19]. Since for $K < K_c$, K^{-1} lies outside \mathcal{C} (Fig. 2b), and the winding number is 0. We conclude that for $K < K_c$, \mathcal{S} has no eigenvalues with positive real parts. Thus, for $K < K_c$, mixing is linearly stable². For $K > K_c$, on the other hand, the winding number is 1. Because of eigenvalues with positive real parts, mixing is unstable for $K > K_c$. As $K \rightarrow K_c + 0$, $\lambda \rightarrow 0+$, and at $K = K_c$, mixing undergoes a pitchfork (PF) bifurcation.

Using (2.31) and (2.33), we compute the eigenfunction (written in ω -variable) corresponding to $\lambda = 0$:

$$\Upsilon_0 = \pi g(0)\delta_0 + i\mathcal{P}_0[g] - \frac{e^{-\xi}}{1-i\omega}g(\omega). \quad (3.6)$$

The first two terms on the right-hand side of (3.6) have singularities at $\omega = 0$. The second term also has a regular component, that is smooth in $\omega \neq 0$. This determines the structure of the PLS bifurcating from the mixing state (Fig. 2c). The delta function on the right-hand side of (3.6) implies that the coherent cluster within the PLS is stationary. The regular component of $i\mathcal{P}_0[g]$ and the third term yield the velocity distribution within the incoherent group. The combination of these two terms yields the velocity distribution within the PLS (Fig. 2d). $K = 0.29$ and $n = 5000$ were used in **d**.

4 A bimodal distribution

In this section, we study (1.1) with bimodal frequency distribution. In this setting we find new bifurcations of mixing: an AH bifurcation and a second PF bifurcation. They result in new patterns that are not present in the unimodal case. In the end of this section, we show that breaking symmetry in a family of bimodal distributions leads to formation of chimera states as in a similar scenario for the classical KM identified in our earlier work [7, 18]. In the numerical experiments presented in this section we use the following family of probability density functions

$$g_{\sigma_1, \sigma_2}^\mu(x) = \frac{1}{2\sqrt{2\pi}} \left\{ \frac{e^{-\frac{(x+\mu)^2}{2\sigma_1^2}}}{\sigma_1} + \frac{e^{-\frac{(x-\mu)^2}{2\sigma_2^2}}}{\sigma_2} \right\}. \quad (4.1)$$

When $\sigma_1 = \sigma_2 =: \sigma$, we collapse indices into one $g_\sigma^\mu := g_{\sigma, \sigma}^\mu$.

4.1 An Andronov-Hopf bifurcation

First, we keep $\sigma_1 = \sigma_2 =: \sigma$ and increase μ from zero. We want to understand how the critical curve changes as μ is varied. The key events in the metamorphosis of \mathcal{C} are shown in Fig. 3e-h. For small $\mu > 0$, \mathcal{C}_μ ³ is diffeomorphic to \mathcal{C}_0 (cf. Fig. 2b) in a neighborhood of P_0 , the point the intersection of \mathcal{C}_0 with the

²In fact, it is asymptotically stable with respect to a suitable weak topology [5].

³From this point on, we explicitly indicate the dependence of \mathcal{C} , x , and P on μ .

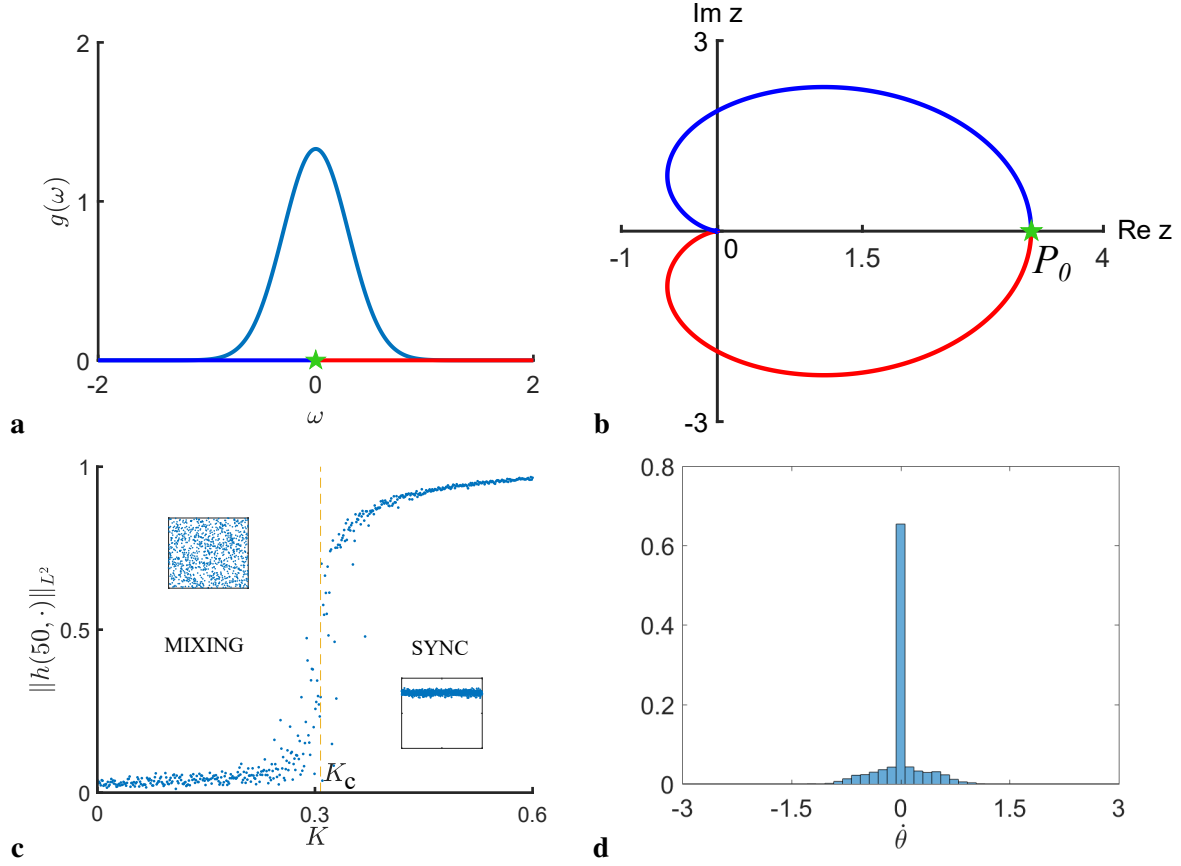


Figure 2: **a**) A graph of an even unimodal probability density function g . We take a Gaussian centered at 0 with $\sigma = 0.3$. **b**) The corresponding critical curve \mathcal{C} intersects positive real semiaxis at a unique point P_0 indicated by a green star. The preimage of P_0 under G is indicated by the green star in **(a)**. **c**) P_0 corresponds to the PF bifurcation of mixing resulting in a PLS, which is then gradually transformed into synchronous state. **d**) The velocity distribution within the PLS near PF bifurcation is determined by the eigenfunction (3.6).

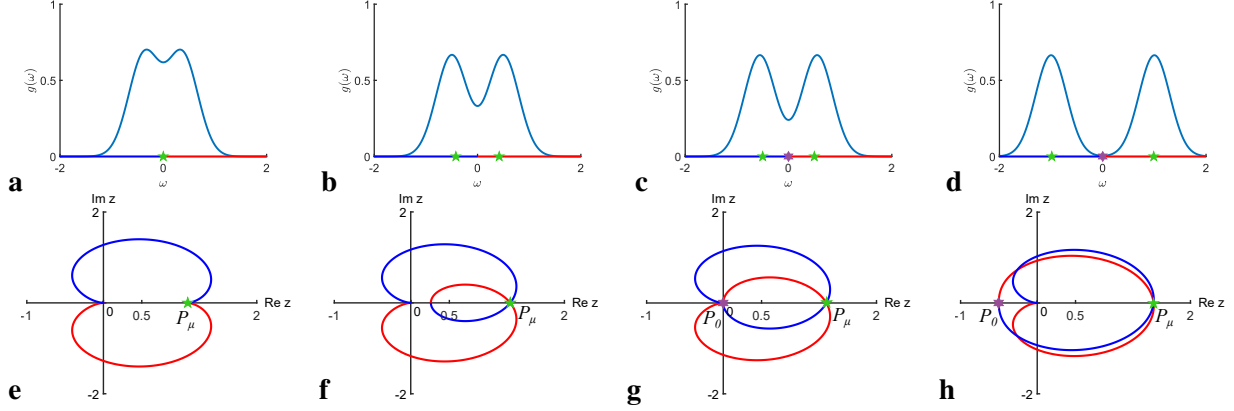


Figure 3: Continuous deformation of the unimodal symmetric density g with $\sigma = 0.3$ into a bimodal symmetric one (a-d) and the plots of the corresponding critical curves (e-h). At the critical value $\mu = \mu^* \approx 0.413$, C_{μ^*} develops a cusp (e). This corresponds to the codimension-2 bifurcation of mixing. The preimages of points of the intersection of the critical curve with the real axis P_0 and P_μ in (e-h) are indicated by stars in the corresponding plots in (a-d). From left to right, μ increases from μ^* to 0.5, 0.555, and 1.

real axis. At a critical value $\mu^* > 0$, C_{μ^*} develops a cusp at P_{μ^*} (see Fig. 3e). To identify the condition for the cusp, we look for the value of μ , at which the condition of the Inverse Function Theorem fails for G . By (3.3) this occurs when $dy/dt|_{t=0} = 0$, i.e.,

$$J[g_\sigma^{\mu^*}] := \frac{dy}{dt}\bigg|_{t=0} = 2 \int_0^\infty \frac{(g_\sigma^{\mu^*})'(s)}{s(1+s^2)} ds = 0 \quad (4.2)$$

(see Fig. 4a).

For $\mu > \mu^*$ there is a point on the real axis P_μ , which has two preimages under G denoted by $\pm i\nu$ (Fig. 3b, f). Thus, for $\mu > \mu^*$ mixing loses stability through the Andronov-Hopf (AH) bifurcation at $K = K_c^+(\mu)$, $\mu > \mu^*$, giving rise to a two-cluster pattern shown in Figure 1 c. At the AH bifurcation, \mathcal{S} has a pair of complex conjugate eigenvalues $\pm i\nu$. The corresponding eigenfunctions written in ω -variable are given by (2.33)

$$\Upsilon_{\pm i\nu} = \pi g(\pm i\nu) \delta_{\pm i\nu} + i \mathcal{P}_{\pm i\nu}[g] - \frac{e^{-\xi}}{1 + i(\pm i\nu - \omega)} g(\omega). \quad (4.3)$$

Tempered distributions $\Upsilon_{i\nu}$ and $\Upsilon_{-i\nu}$ have singularities at $i\nu$ and $-i\nu$ respectively due to δ . and \mathcal{P} . on the right-side of (4.3). This implies the existence of two groups of phase-locked oscillators moving with velocities approximately equal to $\pm\nu$. Moreover, Fig. 4b shows that outside a small neighborhood of μ^* , $\nu \approx \mu$ and so the group velocities correspond to the peaks of the density g_σ^μ . The regular part of \mathcal{P} . results in a cloud of irregularly moving oscillators. This explains the salient features of the two-clusters patterns in the pattern replacing mixing after it loses stability (see Fig. 5a). Note that $\mu = \mu^*$ separates the regions of the PF and AH bifurcations. At this value of μ and the corresponding critical value of K mixing undergoes a codim-2 bifurcation. Unfolding of this bifurcation contains a range of spatiotemporal patterns bifurcating from mixing including one- and (traveling) two- cluster states and chimera states (see Section 4.3).

4.2 A second pitchfork bifurcation

For increasing values of $\mu > \mu^*$, the loop formed by the critical curve grows while remaining in the right half-plane (Fig. 3f). At a certain value $\mu^0 > \mu^*$ it hits the origin (Fig. 3g). For $\mu > \mu^0$ the point of simple intersection of \mathcal{C} with the real axis moves into the negative semiaxis. This corresponds to the creation of the new pitchfork bifurcation at a negative value:

$$K_c^- = \left(\pi g(0) - \int_{-\infty}^{\infty} \frac{g(\omega)}{1 + \omega^2} d\omega \right)^{-1} < 0, \quad (4.4)$$

which leads to a pattern shown in Figure 1 g. Thus, for $\mu > \mu^0$ mixing is stable for $K \in (K_c^-, K_c^+)$ with $K_c^- < 0 < K_c^+$. The corresponding unstable mode at the PF bifurcation at K_c^- is still given by (3.6) albeit with a bimodal g . In the present case, Equation (3.6) implies that there is a group of stationary phase-locked oscillators due to δ_0 and the singularity of $\mathcal{P}_0[g]$ on the right-hand side of (3.6). In addition, there is a group of moving oscillators whose velocities are determined by the regular part of $\mathcal{P}_0[g]$ and the last term on the right-hand side of (3.6).

Equation (3.6) accounts for the velocity distribution of the pattern replacing mixing but it does not explain why the phase-locked oscillators are organized in two antiphase coherent groups whereas for the PF at positive K_{PF} analyzed in Section 3 there is a single coherent group. The splitting into two groups can be understood with the help of the method used in [18] for studying cluster dynamics. We outline the argument from [18] to the extent needed for present purposes. To this end, let

$$J^- := \{j \in [n] : \omega_j < 0\} \quad \text{and} \quad J^+ := \{j \in [n] : \omega_j \geq 0\}$$

and

$$U_1 = |J^-|^{-1} \sum_{i \in J^-} \theta_i \quad \text{and} \quad U_2 = |J^+|^{-1} \sum_{i \in J^+} \theta_i.$$

Here, $|J|$ denotes the cardinality of J . $U_{1,2}$ describe the evolution of the two macroscopic clusters of phase-locked oscillators. In [17] it is shown that in the limit $n \rightarrow \infty$, U_1 and U_2 satisfy the following system of ODEs

$$\begin{aligned} \ddot{U}_1 + \dot{U}_1 &= -\mu + K \sin(U_2 - U_1), \\ \ddot{U}_2 + \dot{U}_2 &= \mu + K \sin(U_1 - U_2), \end{aligned}$$

From this, we derive an ODE for $X = U_2 - U_1$

$$\begin{aligned} \dot{X} &= Y, \\ \dot{Y} &= 2\mu - Y - K \sin X. \end{aligned} \quad (4.5)$$

A standard calculation shows that $(\arcsin(\frac{2\mu}{K}), 0)$ and $(\pi - \arcsin(\frac{2\mu}{K}), 0)$ are two equilibria of (4.5). Furthermore, the former is stable for $K > 0$ and the latter is stable for $K < 0$.

4.3 Chimera states

We now fix $\mu \in (\mu^*, \mu^0)$ and break the even symmetry of g_σ^μ by increasing σ_1 and decreasing σ_2 (see Fig. 6a). This affects the critical curve $\mathcal{C}_{\mu, \sigma_1, \sigma_2}$ in the following way. The point of double intersection P_μ

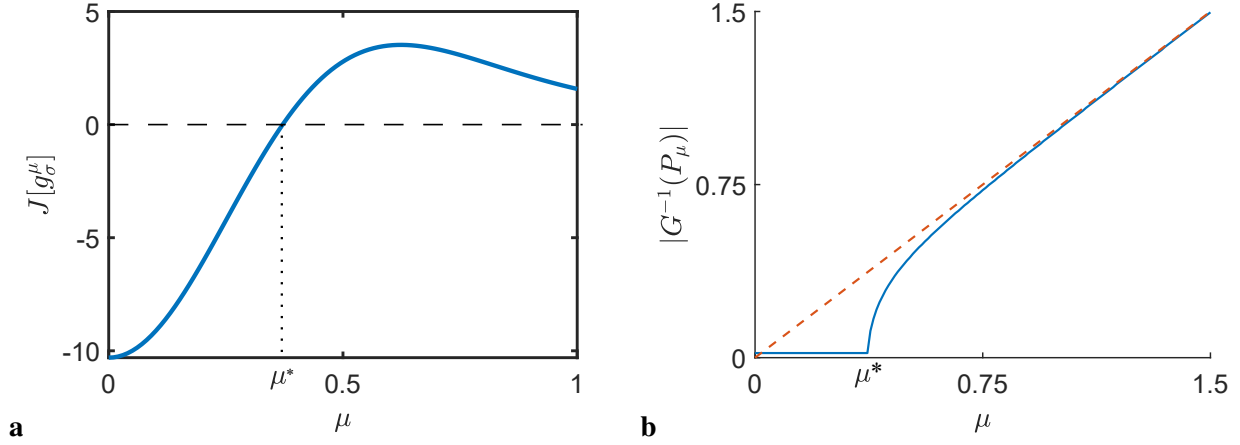


Figure 4: **a)** The plot of $J[g_\sigma^\mu]$ vs μ (cf. (4.2)) when $\sigma = 0.3$. The zero of $J[g_\sigma^\mu]$ determines the critical value μ^* . **b)** The plot of the absolute value of the two preimages $G^{-1}(P_\mu)$. Note that for $\mu > \mu^*$ outside a small neighborhood of μ^* , $|G^{-1}(P_\mu)| \approx \mu$, i.e., the two preimages of P_μ lie near the peaks of the density g_σ^μ . (cf. (4.6)).

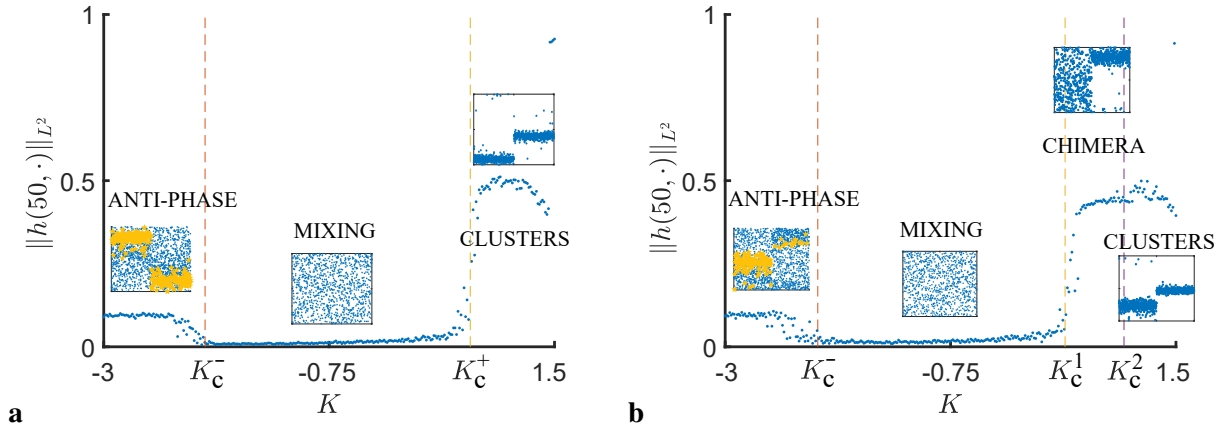


Figure 5: The bifurcation diagrams corresponding to the symmetric and asymmetric bimodal distributions for all-to-all (**a** and **b**, respectively). Colored dots indicate the value of the order parameter computed for each cluster separately for different values of K and different realizations of ω_i 's. To improve visualization, oscillators are rearranged into two groups depending on the sign of their intrinsic frequencies. In (**a**), the loss of stability of mixing at K_c^+ results from the AH bifurcation and so creates a traveling cluster state. In (**b**), a chimera is born at the loss of stability of mixing at K_c^1 . It bifurcates into a moving traveling cluster at K_c^2 . Note that the bifurcations at K_c^1 and K_c^2 affect clusters practically separately. In both cases there is an additional PF bifurcation at $K_c^- < 0$ resulting in stationary, anti-phase clusters. To better visualize this state, all oscillators whose average velocity is sufficient small are colored in yellow stars. The following parameters were used for the distributions of the intrinsic frequencies a) $\sigma = 0.3$, $\mu = 1$; b) $\sigma_1 = 0.4$, $\sigma_2 = 0.2$, $\mu = 1$.

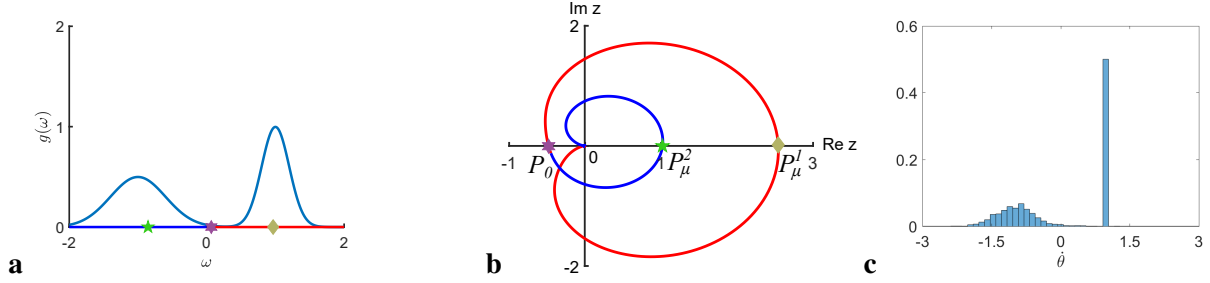


Figure 6: **a)** Asymmetric bimodal distribution with $\sigma_1 = 0.4$, $\sigma_2 = 0.2$, and $\mu = 1$; **b)** its corresponding critical curve. **c)** The histogram of the velocity distribution within a chimera is fully determined by the singular distribution $v_{it_\mu+0}$. The histogram was generated by simulating (1.1) with $n = 5000$, $K = 0.75$.

splits into two points of intersection with the real axis: $P_\mu^1 = (x_\mu^1, 0)$ and $P_\mu^2 = (x_\mu^2, 0)$ with $0 < x_\mu^2 < x_\mu^1$ (see Fig. 6b). Note that the preimages of these points under G are still very close to the maxima of $g_{\sigma_1, \sigma_2}^\mu$ (see Fig. 6a). In particular, the preimage of P_μ^1 is approximately $i\mu$, the center of the more localized peak of $g_{\sigma_1, \sigma_2}^\mu$. This implies that mixing loses stability at $K_c^1 \approx G(i\mu)^{-1}$. The bifurcating eigenvalue $\lambda = i\nu_1$ ($\nu_1 \approx \mu$) and the corresponding eigenfunction

$$\Upsilon_{i\nu_1} = \pi g_{\sigma_1, \sigma_2}^\mu(\nu_1) \delta_{\nu_1} + i\mathcal{P}_{\nu_1}[g_{\sigma_1, \sigma_2}^\mu] - \frac{e^{-\xi} g_{\sigma_1, \sigma_2}^\mu(\omega)}{1 + i(\nu_1 - \omega)}. \quad (4.6)$$

Note that the first term on the right hand side of (4.6) is a singular distribution localized at ν_1 . The second term has a singularity at ν_1 , but its regular part has some ‘weight’ near $\nu_2 \approx -\mu$. These features translate into the velocity distribution within a chimera: there is a tightly localized peak around μ (the coherent group) and a broader peak near $-\mu$ (the incoherent group) (Figs. 6c and 5b).

5 The role of connectivity: nearest-neighbor coupling

We have seen above that a PF bifurcation of mixing results in the formation of one or a pair of stationary coherent clusters depending on the distribution type and the sign of K , while the AH bifurcation leads to a pair of travelling coherent structures. All these patterns are spatially homogeneous if the coupling is all-to-all, because the only nonzero eigenvalue of \mathbf{W} is positive and the corresponding eigenfunction is constant. In general, \mathbf{W} may have eigenvalues of both signs [4]. In this case, the interval of stability of mixing is bounded from both sides (K_c^-, K_c^+) , $K_c^- < 0 < K_c^+$. The values of K_c^- and K_c^+ , as well as the types of the bifurcations at these values of K , depend on the interplay between the type of the distribution of ω_i and the spectral properties of \mathbf{W} . Furthermore, the bifurcation at one of these points results in a pattern with nontrivial spatial structure. In this section, we illustrate some of possible bifurcation scenarios by considering (1.1) with a nonlocal nearest-neighbor coupling.

Let $W(x, y) = U(x - y)$, which is defined by

$$U(x) = \mathbf{1}_{(-r, r)}(x), \quad \text{on } (-1/2, 1/2)$$

and extended to \mathbb{R} by periodicity. Here, $\mathbf{1}_A$ stands for the indicator function, and $r \in (0, 1/2)$ is a fixed

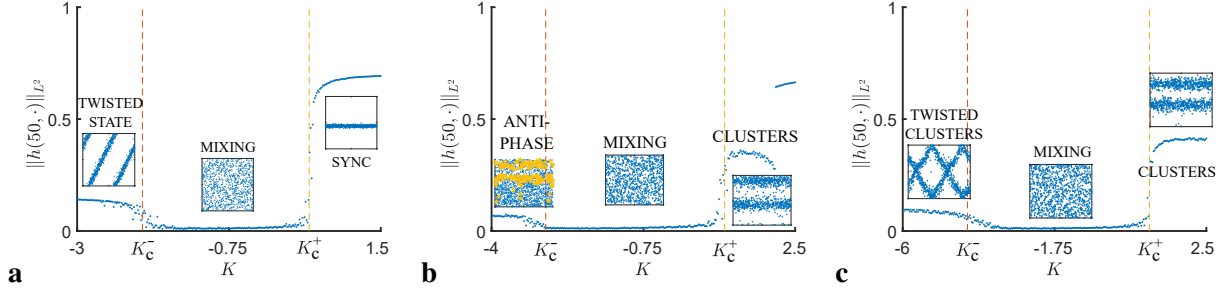


Figure 7: Bifurcation diagrams for (1.1) with unimodal and bimodal intrinsic frequency distributions and nearest neighbor coupling with range $r = 0.35$. For this coupling type, \mathbf{W} has eigenvalues of both signs, i.e., $\nu^- < 0 < \nu^+$. **(a)** For the unimodal distribution ($\sigma = 0.3$) the critical curve has a (simple) intersection with the real axis at $x^+ > 0$ resulting in bifurcations $K_c^- = -\frac{1}{\nu^- x^+}$ (stationary twisted states) and $K_c^+ = \frac{1}{\nu^+ x^+}$ (synchronization). **(b)** For the bimodal distribution ($\sigma_1 = \sigma_2 = 0.3$, $\mu = 1$) the critical curve has two intersections with the real axis, $x^- < 0 < x^+$ (where x^- results in a PF and x^+ in an AH bifurcation). In this case $K_c^- = -\frac{1}{\nu^+ x^-}$ (stationary, anti-phase clusters) and $K_c^+ = \frac{1}{\nu^+ x^+}$ (moving homogeneous clusters). **(c)** Varying the bimodal distribution ($\sigma_1 = \sigma_2 = 0.3$, $\mu = 2$) changes the roots of the critical curve. In this case $K_c^- = -\frac{1}{\nu^- x^+}$ (moving twisted clusters) and $K_c^+ = \frac{1}{\nu^+ x^+}$ (moving homogeneous clusters).

parameter. Then

$$\mathbf{W}[f](x) = \int_{-1/2}^{1/2} U(x-y)f(y)dy.$$

The eigenvalues of \mathbf{W} can be computed explicitly

$$\nu_k = \int_{-1/2}^{1/2} U(x)e^{\pm 2\pi i k x} dx = \int_{-1/2}^{1/2} U(x) \cos(2\pi k x) dx, \quad k = 0, 1, 2, \dots$$

The corresponding eigenfunctions are $w_k = e^{\pm 2\pi i k x}$. The largest positive eigenvalue is $\nu^+ := \nu_0 = 2r$ (cf. [4, Lemma 5.3]). Since $k = 0$, the corresponding eigenspace is 1-dimensional consisting of constant functions. By $k^* > 0$ denote the value of k corresponding to the smallest negative eigenvalue of \mathbf{W} , $\nu^- := \nu_{k^*}$. The corresponding eigenfunctions are $e^{2\pi i k^* x}$ and $e^{-2\pi i k^* x}$.

To explain the implications of the presence of the eigenvalues of both signs in the spectrum of \mathbf{W} , we first turn to the unimodal distribution. If g is even and unimodal then the region of stability of mixing is a bounded interval (K_c^-, K_c^+) with $K_c^- = (\pi g(0)\nu^-)^{-1}$ and $K_c^+ = (\pi g(0)\nu^+)^{-1}$ [4]. At K_c^+ we observe a familiar scenario of transition to synchronization (Figure 7a). At K_c^- the situation is different. The center subspace of the linearized problem in the Fourier space is spanned by

$$v_{\nu^-}^{(1)} = \Upsilon_0(\omega, \xi)e^{2\pi i k^* x} \quad \text{and} \quad v_{\nu^-}^{(2)} = \Upsilon_0(\omega, \xi)e^{-2\pi i k^* x}.$$

In the solution space, we therefore expect that

$$\begin{aligned} f(t, \theta, \psi, \omega, x) &\sim \operatorname{Re} \left\{ \int_{\mathbb{R}} e^{i(\theta - \zeta)} \left(c_1 v_{\nu^-}^{(1)} + c_2 v_{\nu^-}^{(2)} \right) d\zeta, \right\} \\ &= \operatorname{Re} \left\{ \left(c_1 e^{i(2\pi k^* x + \theta)} + c_2 e^{i(-2\pi k^* x + \theta)} \right) \tilde{\Upsilon}_0(\omega, \psi) \right\}, \quad c_1, c_2 \in \mathbb{C}, \end{aligned} \quad (5.1)$$

and

$$\tilde{\Upsilon}_0(\omega, \psi) = \int_{\mathbb{R}} e^{-i\zeta\psi} \Upsilon_0(\omega, \xi(\zeta)) d\zeta.$$

For the PLS emerging at the bifurcation, we see that the structure encoded in $\tilde{\Upsilon}_0(\omega, \psi)$ is now superimposed onto a linear combination of $\pm k^*$ -twisted states (Fig. 7a).

The same principle applies to the analysis of bifurcations in the bimodal case. Suppose μ and σ are such that the critical curve has the form as shown in Figure 3h. Recall that $x^- < 0 < x^+$ denote the x -coordinates of the points of intersection of the critical curve with real axis, P_0 and P_μ . The former is a simple intersection point and the latter is a double intersection point. The expression for x^- is known explicitly

$$x^- = \pi g(0) - \int_{-\infty}^{\infty} \frac{g(\omega)}{1 + \omega^2} d\omega. \quad (5.2)$$

As in the unimodal case, mixing is stable in a finite interval for K , (K_c^-, K_c^+) . The values of K_c^- and K_c^+ as well as the types of the bifurcations at these points depend on x^- , x^+ , ν^- , and ν^+ :

$$K_c^- = -\min \left\{ \frac{1}{|\nu^+ x^-|}, \frac{1}{|\nu^- x^+|} \right\} \quad \text{and} \quad K_c^+ = \min \left\{ \frac{1}{\nu^+ x^+}, \frac{1}{\nu^- x^-} \right\}. \quad (5.3)$$

Here, the type of the intersection at x^\pm (simple vs double) determines the type of the bifurcation, while the eigenfunctions V^\pm corresponding to ν^\pm determine the spatial organization of the emerging pattern (homogeneous vs twisted states). Note that each of the two possible values of K_c^- and K_c^+ in (5.3) corresponds to a distinct combination of the velocity distribution and the spatial profile of the emerging pattern. This results in a four distinct bifurcation scenarios for the loss of stability of mixing in the KM with symmetric bimodal intrinsic frequency distribution.

To illustrate different bifurcation scenarios, we use the following examples. Suppose $|\nu^+ x^-| > |\nu^- x^+|$ then $K_c^- = (\nu^+ x^-)^{-1}$. Because x^- is a simple intersection point, the corresponding bifurcation is PF. The anti-phase solution bifurcating from mixing at $K = K_c^-$ is shown in Fig. 7b (compare with the anti-phase solution in Fig. 5b). Alternatively, if $|\nu^+ x^-| < |\nu^- x^+|$ then $K_c^- = (\nu^- x^+)^{-1}$. This time the bifurcation is AH and the bifurcating pattern are two sets of traveling twisted states (Fig. 7c).

Likewise, there are two possible scenarios for the bifurcations at $K = K_c^+$. If $\nu^+ x^+ > \nu^- x^-$ then $K_c^+ = (\nu^+ x^+)^{-1}$. Thus, we have an AH bifurcation producing two sets of traveling clusters (Fig. 7c). If, on the other hand, $\nu^+ x^+ < \nu^- x^-$ then $K_c^+ = (\nu^- x^-)^{-1}$. The corresponding bifurcation is PF producing a set of stationary twisted states. To illustrate the last scenario, we take

$$U(x) = 2\nu \cos(2\pi x).$$

With this choice of U , the only nonzero eigenvalue of \mathbf{W} is ν . Taking $\nu < 0$ we have $\nu^- = \nu$ and ν^+ does not exist.

The bifurcation at $K_c^- = -\frac{1}{|\nu^- x^+|}$ generates moving twisted clusters, while that at $K_c^+ = \frac{1}{\nu^- x^-}$ results in a pair of stationary antiphase twisted states. These patterns are shown in Figure 8.

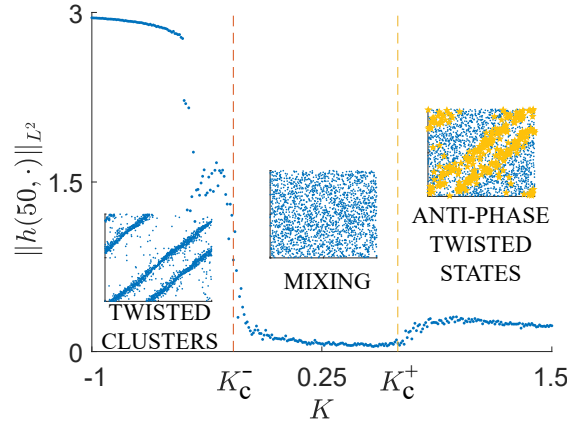


Figure 8: Bifurcation diagram for the coupling $U(x) = -6 \cos(2\pi x)$. Taking bimodal distribution ($\sigma_1 = \sigma_2 = 0.3$, $\mu = 1$) results in the bifurcations $K_c^- = -\frac{1}{|\nu^- x^+|}$ (moving twisted clusters) and $K_c^+ = \frac{1}{\nu^- x^-}$ (stationary, anti-phase twisted states). To better visualize this latter state, the position of every oscillator whose average velocity is sufficiently small is depicted by a yellow star.

6 Discussion

The instability of mixing in the original KM and in the model with inertia reveals a wealth of spatiotemporal patterns in these models. In our previous work [7, 18], we developed a method for studying these patterns, which is based on the combination of the linear stability analysis of mixing (cf. [4]) and Penrose diagrams [19] (see also [8]). In the present paper, we extend this approach to the KM with inertia. We show that in addition to a PF and an AH bifurcations of mixing similar to those analyzed in [7, 18], the KM with inertia features new bifurcation scenarios which were not present in the original model in similar settings. In particular, for the model with symmetric bimodal frequency distribution we identify a new PF bifurcation which follows the AH bifurcation of mixing. The new PF bifurcation results in a new PLS, which consists of two stationary clusters superimposed onto a cloud of irregularly moving oscillators (Fig. 1 g). Note that in the original KM clusters are born in an AH bifurcation and are automatically traveling (cf. [18]). The same bifurcation in the model with inertia on nonlocal nearest neighbor graphs produces similar patterns with coherent clusters organized as twisted states (Fig. 1 f). These patterns were not present in the analysis of the original KM. Furthermore, the presence of the second PF bifurcation enriches the repertoire of possible bifurcation scenarios considerably. For instance, in the model with a family of symmetric bimodal distributions we find four distinct bifurcation scenarios of mixing (cf. Section 5) versus a single bifurcation scenario found for the original KM in a similar setting. This underscores the flexibility of pattern forming mechanisms in the model with inertia.

In addition to applications to biological systems well-known for the ordinary KM, the model with inertia is also known for its applications in modeling power grids [10]. In particular, the model with bimodal frequency distribution comes up in the context of certain high-voltage power grids (cf. [25]). Therefore, bifurcations of mixing identified in the present paper may be useful for understanding stability of these technological systems.

Acknowledgements. This work was supported by JST Moonshot Research and Development grant No. JPMJMS2023 (to HC), NSF grant DMS 2009233 (to GSM), and by Support of Scholarly Activities Grant at The College of New Jersey (to MSM). Numerical simulations were completed using the high performance computing cluster (ELSA) at the School of Science, The College of New Jersey. Funding of ELSA is provided in part by NSF OAC-1828163.

Data availability statement. Data sharing is not applicable to this article as no datasets were generated or analysed during the current study.

References

- [1] J. A. Acebrón, L. L. Bonilla, and R. Spigler, *Synchronization in populations of globally coupled oscillators with inertial effects*, Phys. Rev. E **62** (2000), 3437–3454.
- [2] Hayato Chiba, *A proof of the Kuramoto conjecture for a bifurcation structure of the infinite-dimensional Kuramoto model*, Ergodic Theory Dynam. Systems **35** (2015), no. 3, 762–834.
- [3] ———, *A Hopf bifurcation in the Kuramoto-Daido model*, Journal of Differential Equations **280** (2021), 546–570.
- [4] Hayato Chiba and Georgi S. Medvedev, *The mean field analysis of the Kuramoto model on graphs I. The mean field equation and transition point formulas*, Discrete Contin. Dyn. Syst. **39** (2019), no. 1, 131–155.
- [5] ———, *Stability and bifurcation of mixing in the Kuramoto model with inertia*, SIAM Journal on Mathematical Analysis **54** (2022), no. 2, 1797–1819.
- [6] Hayato Chiba, Georgi S. Medvedev, and Matthew S. Mizuhara, *Bifurcations in the Kuramoto model on graphs*, Chaos **28** (2018), no. 7, 073109, 10.
- [7] Hayato Chiba, Georgi S. Medvedev, and Matthew S. Mizuhara, *Instability of mixing in the Kuramoto model: From bifurcations to patterns*, Pure and Appl. Func. Anal. **7** (2022) no. 4, 1159–1172.
- [8] Helge Dietert, *Stability and bifurcation for the Kuramoto model*, J. Math. Pures Appl. (9) **105** (2016), no. 4, 451–489.
- [9] R. L. Dobrušin, *Vlasov equations*, Funktsional. Anal. i Prilozhen. **13** (1979), no. 2, 48–58, 96.
- [10] Florian Dörfler and Francesco Bullo, *Synchronization and transient stability in power networks and nonuniform Kuramoto oscillators*, SIAM J. Control Optim. **50** (2012), no. 3, 1616–1642.
- [11] François Golse, *On the dynamics of large particle systems in the mean field limit*, Macroscopic and large scale phenomena: coarse graining, mean field limits and ergodicity, Lect. Notes Appl. Math. Mech., vol. 3, Springer, [Cham], 2016, pp. 1–144.
- [12] Shamik Gupta, Alessandro Campa, and Stefano Ruffo, *Nonequilibrium first-order phase transition in coupled oscillator systems with inertia and noise*, Phys. Rev. E **89** (2014), 022123.

- [13] Peron T. Rodrigues F.A. Kurths J. Ji, P., *Low-dimensional behavior of kuramoto model with inertia in complex networks*, Sci. Rep. **4** (2014), 4783.
- [14] Dmitry Kaliuzhnyi-Verbovetskyi and Georgi S. Medvedev, *The mean field equation for the Kuramoto model on graph sequences with non-Lipschitz limit*, SIAM Journal on Mathematical Analysis **50** (2018), no. 3, 2441–2465.
- [15] Yoshiki Kuramoto, *Self-entrainment of a population of coupled non-linear oscillators*, International Symposium on Mathematical Problems in Theoretical Physics (Kyoto Univ., Kyoto, 1975), Springer, Berlin, 1975, pp. 420–422. Lecture Notes in Phys., 39.
- [16] Georgi S. Medvedev, *The continuum limit of the Kuramoto model on sparse random graphs*, Commun. Math. Sci. **17** (2019), no. 4, 883–898.
- [17] Georgi S. Medvedev and Mathew S. Mizuhara, *Stability of clusters in the second-order Kuramoto model on random graphs*, J. Stat. Phys. **182** (2021), no. 2, Paper No. 30, 22.
- [18] Georgi S. Medvedev and Matthew S. Mizuhara, *Chimeras unfolded*, J. Stat. Phys. **186** (2022), no. 3, Paper No. 46, 19.
- [19] Oliver Penrose, *Electrostatic instabilities of a uniform non-maxwellian plasma*, The Physics of Fluids **3** (1960), no. 2, 258–265.
- [20] Francisco A. Rodrigues, Thomas K. DM. Peron, Peng Ji, and Jurgen Kurths, *The Kuramoto model in complex networks*, Physics Reports **610** (2016), 1 – 98, The Kuramoto model in complex networks.
- [21] F. Salam, J. Marsden, and P. Varaiya, *Arnold diffusion in the swing equations of a power system*, IEEE Transactions on Circuits and Systems **31** (1984), no. 8, 673–688.
- [22] Barry Simon, *Basic complex analysis*, A Comprehensive Course in Analysis, Part 2A, American Mathematical Society, Providence, RI, 2015.
- [23] Steven H. Strogatz and Renato E. Mirollo, *Stability of incoherence in a population of coupled oscillators*, J. Statist. Phys. **63** (1991), no. 3-4, 613–635.
- [24] Hisa-Aki Tanaka, Allan J. Lichtenberg, and Shin’ichi Oishi, *First order phase transition resulting from finite inertia in coupled oscillator systems*, Phys. Rev. Lett. **78** (1997), 2104–2107.
- [25] Liudmila Tumash, Simona Olmi, and Eckehard Schöll, *Stability and control of power grids with diluted network topology*, Chaos: An Interdisciplinary Journal of Nonlinear Science **29** (2019), no. 12, 123105.